第33卷第1期
2014年2月

红外与毫米波学报
J. Infrared Millim. Waves

Vol. 33, No. 1
February, 2014

文章编号：1001－9014(2014)01－0084－06

DOI：10.3724/SP.J.1010.2014.00084

Higher order distortion calibration model of the internal parameters of star tracker camera with the night sky observation

WANG Fang, LIU Hai-Bo, WANG Zhen-Guo

(College of Aerospace Science and Engineering, National University of Defense Technology, Changsha 410073, China)

Abstract: With the high accuracy of the stellar angular positions, the camera calibration with the night sky observation is available and indispensable. In order to estimate the camera parameters even with higher order nonlinear distortions, a two-step model and the corresponding iterative optimization based on the invariability of inter-star angle were developed in this paper. Furthermore, a compact recursive average filter was designed to improve the accuracy while not adding significantly computation time. The experimental results demonstrated that the proposed model can implement star tracker camera calibration with higher accuracy than the known method.

Key words: star tracker; calibration; higher order distortion; inter-star angle; recursive filter

PACS: 7.68. +m

星敏感器高阶畸变的观星标定模型

王 芳, 刘海波, 王振国

(国防科学技术大学 航天科学与工程学院,湖南 长沙 410073)

摘要：由于恒星具有很高的姿态精度，使得观星标定成为星敏感器相机参数标定中不可缺少的一种方法.针对高阶非线性畸变情况下的星敏感器相机参数标定问题进行研究，基于星间距的不变性建立了一个两步标定模型.设计了一个紧致的递归均值滤波器来进行参数估计，该滤波器可以在不显著增加计算量的情况下提高参数估计的精度.实验结果表明，相比已有方法，所提出的方法能够实现更高精度的星敏感器相机标定.

关 键 词：星敏感器;标定;高阶畸变;星间角;递归滤波

中图分类号：P236 **文献标识码**：A

Introduction

Star trackers can provide high precise attitude parameters of the spacecrafts without prior knowledge, which makes them the super-choice devices for small satellites[1, 2]. The precision of the observed star directions is mainly determined by the star tracker camera parameters, i. e. the focal length f, the principal point(x_0, y_0), and the distortion parameters which usually are calibrated on the ground before launching[3].

Generally, two distinct types of approaches, i. e. the indoor stellar simulation and the night sky observation are processed to acquire the calibration data. In the indoor stellar simulation approach, simulated star lights with preset incidence angles and calibration patterns with Euclidean structures are achieved as the calibrated control points[4-7]. The absolute precision of these methods is about $0.01 \sim 0.07$deg$(1.7 \times 10^{-4} \sim 12.2 \times 10^{-4}$ rad$)$. However, the traditional laboratory

Received date: 2012 - 11 - 12, **revised date**: 2013 - 10 - 10 **收稿日期**: 2012 - 11 - 12, **修回日期**: 2013 - 10 - 10

Foundation items: Supported by National Natural Science of China(61205190).

Biography: Wang Fang(1981-), Female, Gaoping, Shanxi, master. Research area involves Image processing, error modeling and calibration. E-mail: fangw1981_2010@163. com.

calibration method requires high precise rotation platforms, collimators, and star point plates, which are usually expensive and complex. Contrariwise, the real night sky observation on the ground can acquire the calibration data perfectly without expensive setups[8]. Recently, we have presented a two-step calibration approach depending upon the dot-product[9]. In this paper, we develop the two-stage camera calibration model of higher order distortion, which can be realized even for single image. Furthermore, a compact recursive average filter is designed to increase the accuracy while not adding significantly computation work and time. The experimental results demonstrated that the proposed model can implement star tracker camera calibration with high accuracy.

1 Mathematical model for ground-based calibration

1.1 Distortion-free camera model

For a pinhole imaging system, the object-image relation of the star tracker is determined by the linear projection relation as shown in Fig. 1. The translation vector can be neglected since the distance to the star tracker is significantly less than the distance to a star in the inertial frame. Therefore, the angle θ_{ij} between the direction vectors of two stars is invariant in star tracker frame and inertial frame[10]. That is to say, the angle between w_i and w_j equals to the angle between v_i and v_j, where w_i and w_j are the direction vectors of star i and star j in star tracker frame, respectively, and v_i and v_j are the direction vectors of star i and star j in inertial frame, respectively.

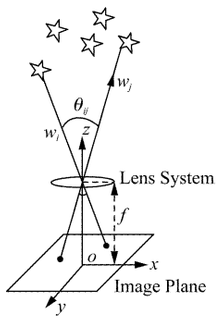

Fig. 1　Measurement model of star tracker
图 1　星敏感器测量模型

The dot product method is widely adopted to learn the calibration corrections of the focal length and principal point[9-11], in which the observation equations can be constructed as following

$$\cos\theta_{ij} = v_i^T v_j = w_i^T w_j \quad , \quad (1)$$

where $i = 1, 2, \ldots, n-1$; $j = i+1, i+2, \ldots, n$. v and w represent the direction vector in the inertial frame and the star tracker frame, respectively, which can be expressed as

$$v = \begin{bmatrix} \cos\alpha\cos\delta \\ \sin\alpha\cos\delta \\ \sin\delta \end{bmatrix} \quad , \quad (2)$$

and

$$w = \frac{1}{\sqrt{(x-x_0)^2 + (y-y_0)^2 + f^2}} \begin{bmatrix} -(x-x_0) \\ -(y-y_0) \\ f \end{bmatrix} . \quad (3)$$

In Eq. (2-3), (α, δ) represents the right ascension and declination of the associated guide star; f, (x_0, y_0) and (x, y) represent the focal length, principal point and observed star location in the detector image plane, respectively.

By expanding Eq. (1) with Eq. (3) for both measured vectors, the following expression can be achieved:

$$v_i^T v_j = \frac{N_{ij}}{D_i D_j} = F_{ij}(x_0, y_0, f) \quad , \quad (4)$$

where

$$\begin{cases} N_{ij} = (x_i - x_0)(x_j - x_0) + (y_i - y_0)(y_j - y_0) + f^2 \\ D_i = \sqrt{(x_i - x_0)^2 + (y_i - y_0)^2 + f^2} \\ D_j = \sqrt{(x_j - x_0)^2 + (y_j - y_0)^2 + f^2} \end{cases} . \quad (5)$$

1.2 Higher order distortion consideration model

As a result of several types of imperfections in the design and assembly of the camera optical system, the expressions in Eq. (4) don't hold true always. Weng *et al*. introduced a camera model considering radial, decentering, and thin prism distortions in Ref. 12. According to Weng's model, the star position must be replaced by the expressions that explicitly take into account the positional error[12]

$$\begin{bmatrix} x' \\ y' \end{bmatrix} = \begin{bmatrix} x \\ y \end{bmatrix} - \begin{bmatrix} \delta x \\ \delta y \end{bmatrix} = \begin{bmatrix} x \\ y \end{bmatrix} - \begin{bmatrix} (g_1 + g_3)u^2 + g_4 uv + g_1 v^2 + \kappa u(u^2 + v^2) \\ g_2 u^2 + g_3 uv + (g_2 + g_4)v^2 + \kappa v(u^2 + v^2) \end{bmatrix} . \quad (6)$$

In Eq. (6), x' and y' are the non-observable and distortion-free image coordinates; x and y are the observable coordinates with distortion. $u = x - x_0$, $v = y - y_0$, $g_1 = s_1 + p_1$, $g_2 = s_2 + p_2$, $g_3 = 2p_1$, and $g_4 = 2p_2$, where s_1 and s_2 represent the thin prism distortion, $p_1$and p_2 represent the decentering distortion, κ represents the radial distortion.

Thus, Eq. (5) should be rewritten as

$$\begin{cases} N_{ij} = (x_i - x_0 - \delta x_i)(x_j - x_0 - \delta x_j) + \\ \quad (y_i - y_0 - \delta y_i)(y_j - y_0 - \delta y_j) + f^2 \\ D_i = \sqrt{(x_i - x_0 - \delta x_i)^2 + (y_i - y_0 - \delta y_i)^2 + f^2} \\ D_j = \sqrt{(x_j - x_0 - \delta x_j)^2 + (y_j - y_0 - \delta y_j)^2 + f^2} \end{cases} . \quad (7)$$

For the star trackers with high accuracy, calibration procedures should not only determine the focal length and principal point values, but also accurately identify the distortion model.

1.3 Intersect direction iteration parameter estimation

The parameter estimation can be realized by the following intersect direction iteration:

Step 1. Estimate the optimal principal point and focal length with fixed distortion parameters.

The estimated value of principal point and focal length can be achieved by performing a first-order Taylor series expansion on the nonlinear function $F_{ij}(\hat{x}_0, \hat{y}_0, \hat{f})$.

$$\begin{bmatrix} x_0 \\ y_0 \\ f \end{bmatrix} = \begin{bmatrix} \hat{x}_0 \\ \hat{y}_0 \\ \hat{f} \end{bmatrix} + (H^T H)^{-1} H^T R \quad , \quad (8)$$

where,

$$H = \begin{bmatrix} \frac{\partial F_{12}}{\partial x_0} & \frac{\partial F_{12}}{\partial y_0} & \frac{\partial F_{12}}{\partial f} \\ \frac{\partial F_{13}}{\partial x_0} & \frac{\partial F_{13}}{\partial y_0} & \frac{\partial F_{13}}{\partial f} \\ \vdots & & \vdots \\ \frac{\partial F_{ij}}{\partial x_0} & \frac{\partial F_{ij}}{\partial y_0} & \frac{\partial F_{ij}}{\partial f} \\ \vdots & & \vdots \\ \frac{\partial F_{n-1,n}}{\partial x_0} & \frac{\partial F_{n-1,n}}{\partial y_0} & \frac{\partial F_{n-1,n}}{\partial f} \end{bmatrix}_{(\hat{x}_0, \hat{y}_0, \hat{f})} ;$$

$$R = \begin{bmatrix} v_1^T v_2 - F_{12}(\hat{x}_0, \hat{y}_0, \hat{f}) \\ v_1^T v_3 - F_{13}(\hat{x}_0, \hat{y}_0, \hat{f}) \\ \vdots \\ v_i^T v_j - F_{ij}(\hat{x}_0, \hat{y}_0, \hat{f}) \\ \vdots \\ v_{n-1}^T v_n - F_{n-1,n}(\hat{x}_0, \hat{y}_0, \hat{f}) \end{bmatrix} , \quad (9)$$

where, $i = 1, \ldots, n-1$; $j = i+1, \ldots, n$; n denotes the number of observations.

Step 2. Estimate the distortion parameters after achieving the other parameters in the first step.

The image plane distortion $(\delta x, \delta y)$ for observable coordinates (x, y) can be expressed as

$$\begin{cases} \delta x = \Phi \hat{a} \\ \delta y = \Phi \hat{b} \end{cases} , \quad (10)$$

where Φ is the basic function describing the focal plane distortions, $\hat{a}$ and $\hat{b}$ are the corresponding coefficients respectively. $\hat{a} = (\hat{g}_1, \hat{g}_2, \hat{g}_3, \hat{g}_4)^T$ $\hat{b} =$,

Thus, the distortions coefficients can be estimated with the principal point and the focal length being fixed according to Eq. (11).

$$\begin{bmatrix} \hat{a} \\ \hat{b} \end{bmatrix} = \begin{bmatrix} \hat{a}_0 \\ \hat{b}_0 \end{bmatrix} + (H_d^T H_d)^{-1} H_d^T R_d \quad , \quad (11)$$

where

$$H_d = \begin{bmatrix} \frac{\partial F_{12}}{\partial \hat{a}} & \frac{\partial F_{12}}{\partial \hat{b}} \\ \frac{\partial F_{13}}{\partial \hat{a}} & \frac{\partial F_{13}}{\partial \hat{b}} \\ \vdots & \vdots \\ \frac{\partial F_{ij}}{\partial \hat{a}} & \frac{\partial F_{ij}}{\partial \hat{b}} \\ \vdots & \vdots \\ \frac{F_{n-1n}}{\partial \hat{a}} & \frac{\partial F_{n-1n}}{\partial \hat{b}} \end{bmatrix}_{(\hat{a}_0, \hat{b}_0)} ;$$

$$R_d = \begin{bmatrix} v_1^T v_2 - F_{12} \\ v_1^T v_3 - F_{13} \\ \vdots \\ v_i^T v_j - F_{ij} \\ \vdots \\ v_{n-1}^T v_n - F_{n-1n} \end{bmatrix}_{(\hat{a}_0, \hat{b}_0)} . \quad (12)$$

Step 3. Step 1 and step 2 will be repeated to improve the estimated values of camera parameters iteratively.

1.4 Recursive average filter for optimization

Generally, the star camera can be calibrated from a single night sky image using the methods mentioned previously. However, there is large variation and uncertainty for calibration with a single image. Thus, the traditional attitude independent methods are performed on a large number of images using a batch process or a recursive least square such as Kalman Filter. In this paper, a compact recursive filter is designed to optimize the estimated results of the single image.

Let Z_k denotes the filter result of the star image marked k, X_{k+1} denotes the estimated result of any one of the calibration methodologies described before with the image marked by $k+1$, the final estimate result of the filter is Z_{k+1}:

$$Z_{k+1} = \beta Z_k + (1-\beta) X_{k+1} \quad . \quad (13)$$

In Eq. (13), the value of β which denoted as $\beta = k/(k+1)$ can be set at the range of 0 ~ 1. In the recursive average filter, the filtering result Z_{k+1} is equal to the average of the estimated results of the total previous k images.

2 Night sky observations for ground-based calibration

2.1 Night sky observation setup

Next, we use the real night sky observation data to obtain the star image.

Suppose that the designed focal length, the FOV and the star magnitude limit are about 105.75 mm, 5.1°(3.6° × 3.6°) and 8.0Mv respectively, and the resolution of the CCD camera is 512 × 512 pixels with pixel pitch of 13 μm × 13 μm.

As the atmosphere has a particular index of refraction, a star will appear higher in the sky than its true position. While the refraction in the direction of the zenith is zero, it changes with an increasing different angle to the zenith direction[13]. In order to reduce the influence of the atmosphere, the optical axis is pointed to the zenith to the utmost during the star observation, in which the maximal difference angle of the star direction in the FOV with the zenith direction is about FOV/2. According to the research results of Smart[14], the effect of the atmosphere refraction is less than 1.3×10^{-5} rad for the designed star tracker with 5.1° FOV.

2.2 Calibration results

With a total number of 1 000 images taken by the observation, a series of image data processes are performed to calibrate the star tracker. To evaluate the effect of the method, the mean and the standard deviation of the estimation results during 0 ~ 200 s are shown in Table 1. According to the results shown in Table 1, there is large variation and uncertainty especially for the distortion parameters and principal point, which may be caused by the following reasons: (1) The number of stars identified as the control points is only about 23 for a single image, which is sparse compared with the image plane of the detector; (2) Compared with the focal length, the distortion parameters and the principal point have larger unobservable nature.

Next, we consider the estimation based on 1 000 images. As shown in Fig. 2, the recursive average filter increases the accuracy remarkable, and the convergence is achieved after about 400 images.

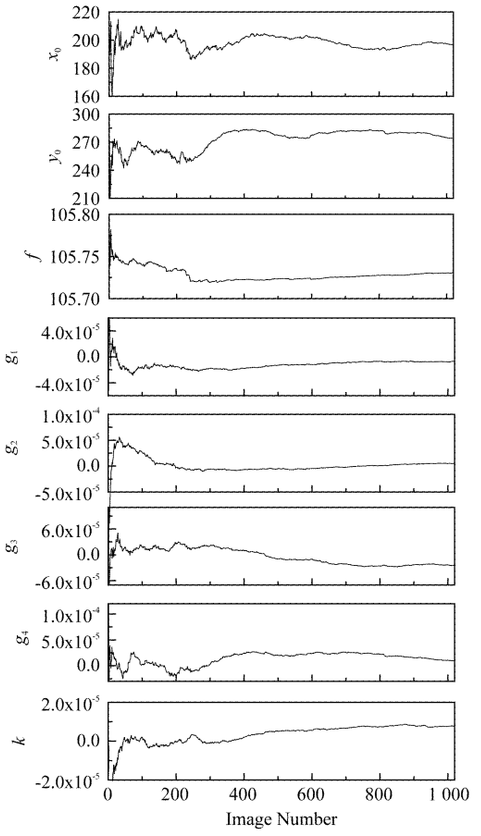

Fig. 2　Estimated results with recursive average filter
图 2　利用递归均值滤波器估计的结果

Table 1 Statistical characteristic of estimated results from single images
表1 基于单幅图像得到的估计结果的统计性质

	x_0(pixels)	y_0(pixels)	f(mm)	g_1	g_2	g_3	g_4	k
Mean	204.82	271.66	105.708	-3.6e-6	7.7e-6	6.2e-6	-8.8e-6	3.6e-7
Stan. Dev.	113.68	118.15	0.050	1.4e-4	1.2e-4	1.8e-4	1.7e-4	3.4e-5

2.3 Error analysis and discussion

Next, the inter-star angles will be analyzed to evaluate the performances of the three calibration approaches. Define deviation $\Delta\theta$ as follows

$$\Delta\theta = |\theta_{measured} - \theta_{ture}| \quad , \quad (14)$$

where $\theta_{measured}$ and θ_{ture} are the measured inter-star angle according to the estimated camera parameters and its true value in the guide star catalog respectively.

The estimations of (x_0, y_0), f and the root mean square(RMS) value of the deviations $\Delta\theta$ were shown in Table 2. RMS is defined as RMS $= \sqrt{\sum_{i=1}^{N} (\Delta\theta_i)^2}$, where N is the number of inter-star angles.

Table 2 Calibration results and their associated deviations of the measured inter-star angles
表2 标校结果及其星角距偏差

	(x_0, y_0)(pixels)		f(mm)	RMS$\Delta\theta$(rad)
Dot Product Method in Ref. 15	163.07	289.87	105.8152	5.23e-5
Scalar Cross Product Method in Ref. 15	163.66	290.83	105.8038	5.13e-5
Two steps' Dot Product Method in Ref. 9	165.88	294.74	105.7831	3.03e-5
Iterative Dot Product Method with recursive average filter	216.79	267.04	105.7335	2.43e-5
Iterative Dot Product Method with Batch Process	216.40	268.33	105.7345	2.35e-5

According to the experimental results, the following items can be put forward:

1. As the camera distortions were not estimated in Ref. 15, the estimated results of Ref. 15 have the maximum deviations.

2. Compared with the two-step calibration approach, the improved method with iterative optimizations can achieve higher accuracy.

3. The estimated results of the recursive average filter are equal to that of the batch process. Compared with the calibration of the single image, this compact filter improve the accuracy remarkably while not consuming significantly more computation time, which can be identified for the autonomous on-orbit calibration of the star tracker camera.

3 Conclusion

The attitude determination accuracy of the star tracker highly depended on the camera parameters. This paper presents a possible methodology to perform camera calibration for star trackers with star observation. Compared with former works, two-step approaches and the corresponding iterative optimization are adopted to estimate the star tracker camera parameters even with nonlinear camera distortions. Furthermore, the recursive average filter is designed to improve the accuracy.

The observing data in the night sky were adopted to test the performance of the calibration approaches. The test results indicate that the two-step approach with iterative optimizations performs well in terms of accuracy. And recursive average filter increases the accuracy remarkable without adding significant computation work and delay into the system. It can also satisfy the autonomous on-orbit calibration of the star tracker camera.

REFERENCES

[1] LIEBE C C. Star trackers for attitude determination[J]. *IEEE Aerospace and Electronic Systems Magazine*, 1995, **10**(6), 10-16.

[2] JU G, KIM H, POLLOCK T, *et al*. DIGISTAR - A low cost micro star tracker: AIAA Space Technology Conference & Exposition, 1999[C]. Albuquerque NM:[s. n.], 1999: 28-30.

[3] PAULSEN T E, MARESI L. Calibration and verification of the TERMA star tracker for the NEMO satellite: AIAA Space 2000 Conference and Exposition, 2000[C]. Long Beach, CA: :[s. n.], 2000: 19-21.

[4] LIU Haibo, LI Xiujian, TAN Jichun, *et al*. Novel approach for laboratory calibration of star tracker[J]. *Optical Engineering*, 2010, **49**(7): 73601-73609.

[5] RUFINO G, MOCCIA A. Laboratory test system for per-

formance evaluation of advanced star sensors[J]. *Journal of Guidance Control and Dynamics*, 2002, **25**(2): 200 - 208.
[6] XING Fei, DONG Ying, YOU Zheng. Laboratory calibration of star tracker with brightness independent star identification strategy[J]. *Optical Engineering*, 2006, **45**(6): 63601 - 63604.
[7] DAVALOS P. Evaluation of Camera Calibration Methods for Star Identification[On-line]. (2007, 12, 01) http://caritags. com/pedro/ davalos_cv_final_ppr_v22. pdf.
[8] KLAUS A, BAUER J, KARNER K, *et al*. Camera calibration from a single night sky image: Proceedings of IEEE Computer Society Conference on Computer Vision and Pattern Recognition, 2004[C]. Washington DC :[s. n.], 2004: 151-157
[9] LIU Haibo J. WANG Jiongqi, TAN Jichun, *et al*. Autonomous on-orbit calibration of a star tracker camera[J]. *Optical Engineering*, 2011, **50**(2): 23604 - 23608.
[10] SAMAAN M A, GRIFFITH T, JUNKINS J L. Autonomous on-orbit calibration of star trackers: Springs: Core Technologies for Space Systems Conference, 2001[C]. *Colorado Springs*, *CO*:[s. n.], 2001: 1 - 18.
[11] GRIFFITH D T, SINGLA P, JUNKINS J L. Autonomous on-orbit calibration approaches for star tracker cameras: Proceeding of Spaceflight Mechanics, 2002[C]. San Antonio, TX:[s. n.], 2002: 39 - 57.
[12] WENG J, COHEN P, HERNIOU M. Camera calibration with distortion models and accuracy evaluation[J]. *IEEE Transactions on Pattern Analysis and Machine Intelligence*, 1992, **14**(10): 965 - 980.
[13] Down D. Image-position error associated with a focal plane array[J]. *J. Opt. Soc. Am. A*, 1992, **9**(5): 700 - 707.
[14] HAGEN N, KUPINSKI M, DERENIAK E L, Gaussian profile estimation in one dimension[J], *Applied Optics*, 2007, **46**(22): 5374 - 5383.
[15] WOODBURY D P, JUNKINS J L. Improving camera intrinsic parameter estimates for star tracker applications: AIAA Guidance, Navigation, and Control Conference, 2009[C]. Chicago: 1 - 11.

(上接 83 页)

as high recall value as RANSAC with much less execution time, which is much better than GTM and BiKNN. Besides, the precision of filtering BiKNN strategy is the highest of all.

REFERENCES

[1] Zitova B, Flusser B. Image registration methods: a survey [J]. *Image and vision computing*, 2003, **21**(11): 977 - 1000.
[2] Liu Z X, An J B, Jing Y. A simple and robust feature point matching algorithm based on restricted spatial order constraints for aerial image registration[J]. *IEEE Transactions on Geoscience and Remote Sensing*, 2012, **50**(2): 514 - 527.
[3] Caetano T S, McAuley J J. Learning graph matching[J]. *IEEE Transactions on Pattern Analysis and Machine Intelligence*, 2009, **31**(6): 1048 - 1058.
[4] Goshtasby A A. 2-D and 3-D image registration: for medical, remote sensing and industrial applications[M]. New Jersey. *John Wiley&Sons Inc*, 2005, 7 - 59.
[5] Dain X, Khorram S. A feature-based image registration algorithm using improved chain-code representation combined invariant moments[J]. *IEEE Transactions on Geoscience and Remote Sensing*, 2005, **43**(9): 2127 - 2137.
[6] Zhang Z X, Li J Z, Li D D. Research of automated image registration technique for infrared images based on optical flow field analysis[J]. *J. Infrared Millim. Waves*(基于光流场分析的红外图像自动配准方法研究, **红外与毫米波学报**), 2003, **22**(4): 307 - 312.
[7] Wen G J, Lv J J, Yu W X. A high-performance feature-matching method for image registration by combining spatial and similarity information[J]. *IEEE Transactions on Geoscience and Remote Sensing*, 2008, **46**(4): 1206 - 1277.
[8] Lowe D G. Distinctive image features from scale-invariant keypoints[J]. *International Journal of Computer Vision*, 2004, **60**(2): 91 - 110.
[9] Fichler M A, Bolles R C. Random sample consensus: a paradigm for model fitting with applications to image analysis and automated cartography[J]. *Communications of the ACM*, 1981, **24**(6): 381 - 395.
[10] Aguilar W, Frauel Y, Escolano F, *et al*. A robust graph transformation matching for non-rigid registration[J]. *Image and vision computing*, 2009, **27**(7): 897 - 910.
[11] Beis J, Lowe D G. Shape indexing using approximate nearest-neighbor search in high-dimensional space[C]. *Proceeding of computer vision and pattern recognition*, Pueto Rico, 1997: 1000 - 1006.
[12] Zhao M, An B, Wu Y, *et al*. Bi-SOGC: A graph Matching Approach based on bilateral KNN Spation Orders around geometric centers for remote sensing image registration[J]. *IEEE Geoscience and Remote Sensing Letters*, 2013, **10**(6): 1429 - 1433.